www.sciencemag.org/cgi/content/full/325/5941/730/DC1

Supporting Online Material for

Unexpected Epoxide Formation in the Gas-Phase Photooxidation of Isoprene

Fabien Paulot,* John D. Crounse, Henrik G. Kjaergaard, Andreas Kürten, Jason M. St. Clair, John H. Seinfeld, Paul O. Wennberg

*To whom correspondence should be addressed. E-mail: paulot@caltech.edu

Published 7 August 2009, *Science* **325**, 730 (2009)
DOI: 10.1126/science.1172910

This PDF file includes:

Materials and Methods
Figs. S1 to S9
Tables S1 to S9
References

Supporting Online Material

Unexpected epoxide formation in the gas-phase photooxidation of isoprene

Fabien Paulot, John D. Crounse, Henrik G. Kjaergaard, Andreas Kürten,
Jason M. St. Clair, John H. Seinfeld, Paul O. Wennberg

Table of content

Chemical ionization mass spectrometer (CIMS)

Overview

The Caltech Chemical Ionization Mass Spectrometer (CIMS) was originally designed for aircraft missions as a robust and lightweight instrument capable of detecting trace amounts of atmospherically-relevant substances with high selectivity and sensitivity. The reagent ion used in negative ion mode, CF_3O^-, reacts with a suite of peroxides and various other compounds, e.g., SO_2, HNO_3 and organic acids (*1-4*).

There exist two versions of the flight instrument: 1) The original version that utilizes a single quadrupole mass filter as a mass spectrometer (*3*) and 2) a more recently developed instrument with the same ionization scheme but utilizing a commercial triple quadrupole mass spectrometer, thereby allowing for the differentiation of certain mass analogues using tandem MSMS. This latter instrument has been largely replicated for laboratory experiments at the Caltech environmental chamber. Additionally, this new instrument can be operated in positive ion mode similar to a classical proton transfer mass spectrometry (PTR-MS) instrument (*5*). The instrument configuration allows for rapid switching between negative and positive ion chemistry. A brief general description of the CIMS follows here with a focus on the MSMS and PTR-MS capabilities, which are key features for the identification of IEPOX formation during isoprene photooxidation, and which have not been described in detail before.

The Caltech CIMS consists of a commercial triple quadrupole mass spectrometer (Varian 300-MS GC/MS, Varian, Inc.) and a custom ion source with a specially designed sample gas inlet system (Fig. S1). During an experiment the sample air is pulled (1 slm) from the chamber through a Teflon line to the instrument. 20% of this sample flow is transferred to the CIMS instrument. The flow rate is controlled by a critical orifice made of glass which connects the sampling line with a 2.54 cm outer diameter glass flow tube coated with a thin layer of Teflon (Fluoropel 801A, Cytonix Corp.). The flow tube is operated at a constant pressure of 35 hPa. The sample flow entering the flow tube is diluted with nitrogen (ultra-high purity, 99.999 %) at a mixing ratio of 1:8.2. The exact value of the dilution flow is adjusted such that the pressure inside the flow tube is held constant at 35 hPa. With the exception of the sample flow, all gas flows are controlled by metal sealed mass flow controllers (SEC-4400, Horiba Stec) to minimize contamination.

The main modification to the Varian triple quadrupole mass spectrometer consists of the removal of the originally installed electron impact ionization source thereby making room for a conically-shaped hexapole ion guide that efficiently transfers ions from the flow tube to the first quadrupole (Q1). The section where the hexapole is mounted is differentially pumped and only connected to the flow tube and the high-vacuum chamber by small openings.

The three linear quadrupole mass filters (Q1, Q2, and Q3) can be used in different configurations allowing either the acquisition of single mass spectra (MS) or tandem mass spectra (MSMS). In the MSMS mode, a buffer gas, nitrogen, is added to the second quadrupole (Q2), which is partially enclosed. In Q2, the presence of several Pa of N_2 results in collision induced dissociation (CID) of the ions selected in Q1. The fragments (or daughter ions) produced in Q2 are filtered by m/z in Q3 before being detected with an electron multiplier operated simultaneously in both analog and ion-counting mode. For the experiments shown here, the following modes were used: (a) Single MS (SMS) -- Operating Q1 as a mass filter to select a single m/z value at a time while operating Q2 (evacuated) and Q3 in RF-only mode such that virtually all ions selected by Q1 reach the detector. In this manner, a mass spectrum can be obtained if all m/z values of interest are scanned (b) MSMS -- Operate Q1 as a mass filter to select a single m/z value for the parent ion. The pressure in the region of Q2 is increased to several Pa inducing the fragmentation of the selected ion. Fragment ions are then selected by Q3 and reach the detector. Mode (a) was conducted for both anions and cations, while mode (b) was conducted for anions only. For the experiments reported in this study, the following sequence was repeated throughout the experiments 1) negative ion SMS, 2) positive ion SMS, and 3) negative ion MSMS, with the total cycle duration being approximately 10 minutes.

Negative ion mode

In negative ion mode, 400 sccm of 10 ppmv CF_3OOCF_3 in N_2 passes through the ion source which contains a radioactive material (^{210}Po foil, NRD, Inc.). The foil containing the ^{210}Po is housed in a stainless steel holder and emits α-particles which by ionizing nitrogen molecules lead to the release of electrons. The electrons are captured by CF_3OOCF_3, generating the reagent anion, CF_3O^-. Potentials of –240 V and -220V (relative to the pinhole and the instrument housing which are held at ground potential) are applied to the stainless steel ^{210}Po holder and –220 V to the lens, respectively, such that only negative ions are transmitted across the flow tube in a transverse direction to the diluted sample flow. Product ions are formed through reactions of neutral analyte molecules with reagent ions as they move across the flow tube. The anions (reagent and product ions) are then pushed towards the pinhole and enter the chamber containing the conical hexapole.

The ion-molecule reactions (with a trace compound R) which can occur are: proton transfer (SR1), fluoride transfer (SR2) or clustering with a CF_3O^- ion (SR3) (*3, 6*)

$$R + CF_3O^- \rightarrow R^- + CF_3OH \qquad \text{(SR1)}$$

$$R + CF_3O^- \rightarrow R^- \bullet HF + CF_2O \qquad \text{(SR2)}$$

$$R + CF_3O^- \rightarrow R^- \bullet CF_3O^- \qquad \text{(SR3)}$$

When operating the instrument in negative SMS mode, anions were scanned sequentially for 0.5 seconds from m/z=50 to m/z=275. The acquisition of a full mass spectrum thus requires ~2 min. The m/z of the reagent anion and its major clusters with water and hydrogen peroxide (m/z=85 (CF_3O^-), m/z=103 ($CF_3O^-\bullet H_2O$) and m/z=119 ($CF_3O^-\bullet H_2O_2$)) are omitted from the scans due to their high intensities; these anions are quantified at m/z +1 – mostly from the ^{13}C isotopologues.

Positive ion mode

In positive ion mode, 400 sccm of N_2 (without CF_3OOCF_3) is passed through the ion source. Residual H_2O in the gas stream reacts with N_2^+ ions (generated from the collisions of the α particles with the bath gas) to form $H^+\bullet(H_2O)_n$ reagent ions in the ion source. The positively charged ions are directed out of the source and across the flow tube by inverting the polarity of the potentials on the ion source and the lens from those used in negative ion mode. The most abundant positive ions detected by the spectrometer correspond to n = 3, 4. The pressure (~3×10^{-3} hPa) inside the conical hexapole limits the transmission of ions with m/z < 50, so that the n=1 and 2 water clusters cannot be detected.

The ion-molecule reactions which occur in positive ion mode are:

$$R + H^+(H_2O)_n \rightarrow R\bullet H^+(H_2O)_x + H_2O_{(n-x)} \qquad \text{(SR4)}$$

where, $x \leq n$, and generally equals 0, 1, or 2.

When operating the instrument in positive SMS mode, ions are scanned sequentially for 0.5 seconds from *m/z*=30 to *m/z*=235. The full mass spectrum requires approximately 1 min and 40s. Ions with *m/z*=55 ($H^+\bullet(H_2O)_3$), *m/z*=73 ($H^+\bullet(H_2O)_4$) are omitted due to their high intensities.

Negative ion MSMS mode

The ion generation for the negative ion MSMS mode is identical to the negative ion SMS mode. The main difference of MSMS mode as compared to the SMS mode is the addition of a small flow of N_2 into the Q2 quadrupole such that the pressure inside Q2 reaches approximately 2.5×10^{-3} hPa. To increase the signal to noise ratio in MSMS mode, the resolution of Q3 is set to a full width half maximum of approximately 1.5 amu. While this does give fairly broad peaks, the chance of distinct fragment ions (excluding isotopic pairs, e.g. ^{12}C and ^{13}C) occurring at adjacent masses (and thus being indistinguishable at this resolution) is small.

In many cases, the formation of the daughter ions induced by collisions of the parent ion (e.g. $R{\bullet}CF_3O^-$) with the bath gas (M) can be explained through the following CID channels:

$R{\bullet}CF_3O^-$ parent ions:

$R{\bullet}CF_3O^- + M \rightarrow CF_3O^- + R + M$ (SR5a)

$R{\bullet}CF_3O^- + M \rightarrow HF{\bullet}R^- + CF_2O + M$ (SR5b)

$R{\bullet}CF_3O^- + M \rightarrow R^-_{-H} + CF_2O + HF + M$ (SR5c)

$R{\bullet}CF_3O^- + M \rightarrow [CF_2O{\bullet}R]^- + HF + M$ (SR5d)

$R{\bullet}CF_3O^- + M \rightarrow HF{\bullet}F^- + HF + CO + R_{-2H} + M$ (SR5e)

$R{\bullet}CF_3O^- + M \rightarrow (HF)_2{\bullet}F^- + CO + R_{-2H} + M$ (SR5f)

$R{\bullet}CF_3O^- + M \rightarrow FCO_2^- + HF + HF + R_{-2H-O} + M$ (SR5g)

$R^-_{-H}{\bullet}HF$ parent ions:

$R^-_{-H}{\bullet}HF + M \rightarrow R^-_{-H} + HF + M$ (SR6)

The distribution across the possible CID channels (SR5a-g) for a given parent ion, $R{\bullet}CF_3O^-$, vary greatly depending upon the nature of R (acidity, fluoride affinity, dipole moment, etc). This distribution can also be modified by changing the average collision energy in Q2, i.e. changing the kinetic energy (velocity) of the ion upon entering Q2. In this work, the ion energies (velocities) are tuned to be quite low (slow) to prevent CID from occurring in the conical hexapole. As a result, it is not possible to alter the collision energies in Q2 significantly without scattering most of the ions onto undetectable trajectories. For a given parent ion m/z, the collisional energy in Q2 was the same across all experiments, and was adjusted as a function of the parent ion mass in order to place the parent ion (and latter the fragment ions) on detectable trajectories, namely those moving through Q2.

The MSMS spectrum of a parent ion is useful for determining the nature of the analyte R as well as distinguishing isobaric compounds which are detected at the same parent m/z. For instance, compounds containing a hydroperoxy group (ROOH) often have a significant yield of the daughter ion at m/z=63 (SR5g), which seems to be a fragment specific to ROOH compounds, probably FCO_2^-. Fingerprints can also be used to distinguish glycolaldehyde from acetic acid. Both compounds are detected at m/z=145 in SMS. In MSMS mode, parent ions arising from acetic acid give daughter ions as m/z=79 (SR5b) with reasonable yield, while parent ions arising from glycolaldehyde do not give any daughter ions at m/z=79. Given calibrated MSMS fragment spectra for acetic acid and glycolaldehyde, one can quantify each compound separately in an unknown mixture.

Experiment

Reagents

All chemicals were purchased from Sigma Aldrich. Atmospheric chamber experiments were carried out in an 800 L FEP Teflon bag filled with ultra zero air (Air Liquide). $H^{18}O^{18}OH$ was purchased from ISOTECH as a 2-3% (by mass) solution in H_2O, and a stated purity of 90% ^{18}O by atom for the H_2O_2. The unlabeled H_2O_2 was prepared as a 3% solution (by mass) using 30% H_2O_2 (Fischer) and deionised water (MilliQue). The concentration of the unlabeled 3% H_2O_2 solution was measured by UV-VIS absorption in the liquid phase after standard dilution using published absorbance cross-sections at 240 nm (7). The concentration and purity of the labeled H_2O_2 was determined to be 2.2% $H^{18}O^{18}OH$ (by mass), and 97.2% ^{18}O (by atom) using the CIMS instrument.

H_2O_2 introduction

A known mass of H_2O_2 (an aliquot of the ~ 3% solutions in H_2O) was evaporated into a 15 SLM stream of ultra zero air (controlled by a mass flow controller) as it filled the 800 L bag. For typical concentrations (1-2 ppmv H_2O_2), the evaporation was complete in 15-20 minutes.

Isoprene introduction

A known mass of isoprene was evaporated into 100 standard liters of N_2 by flowing N_2 over the isoprene and collecting in a 100L Teflon bag. An aliquot (typically 120 mL) from the 100 L isoprene/N_2 mixture was taken using a gas-tight syringe for injection into the 800 L experiment bag. Final isoprene concentration was calculated from the initial mass, and the serial dilution, correcting for the temperature and pressure of the injected aliquot. This procedure was followed prior to each experiment.

Bag flushing

Between experiments, the 800 standard liter experiment bag was flushed with dry N_2 (taken from liquid N_2 boil off). Flushing typically consisted of 4-6 fill and evacuation cycles. After 4 fill/evacuation cycles, all detected compounds are less than 5% of their value at the end of the previous experiment.

Photolysis

The 800 L bag was placed on the floor of the Caltech environmental chamber (8) between the existing 28 m^3 bags. All experiments were conducted using 50% of the UV lights corresponding to $J(H_2O_2)=2.15\times10^{-6}$ s^{-1} (need to modify this). The ambient temperature was between 290 and 295K.

Initial conditions

Three different experiments were carried out with labeled hydrogen (Table S1). The initial concentration of NO_x was determined using the isoprene nitrate cluster signal at m/z=234 and the yields as determined in our earlier work (*6*).

Synthesis of BEPOX

Cis-2,3-epoxy-1,4-butanediol (BEPOX) was synthesized by mixing cis-butene-1,4-diol and hydrogen peroxide under basic conditions and in the presence of tungstinic acid in a 50C water bath (9). The final product was purified by recrystallization from hexanes.

Reactive uptake of BEPOX: Characterization of particle-phase reaction products and their implications for isoprene SOA

Chamber experiments were conducted in order to evaluate the SOA formation potential resulting from the reactive uptake of BEPOX in the presence of acidified sulfate aerosol.

Reactive uptake of BEPOX was monitored via CIMS at m/z=189. Gas-phase BEPOX is largely consumed following addition of the acidic aerosol ($MgSO_4$) to the chamber. The resulting SOA produced from this reaction were collected onto Teflon filters (PALL Life Sciences, 47 mm diameter, 1.0 μm pore size, teflo membrane) for off-line detailed chemical characterization efforts. Tetrols (i.e., erythritol and threitol) were characterized by GC/MS with prior trimethylsilylation (*10*). Additionally, organosulfates (e.g., C_4-trihydroxy sulfates) of BEPOX were characterized by ultra performance liquid chromatography (UPLC) interfaced to an electrospray ionization (ESI) time-of-flight mass spectrometer (TOFMS) operated in the negative ion mode. Details of the Teflon filter extractions and subsequent UPLC/ESI-TOFMS analysis can be found elsewhere (*11*).

The tetrols and organosulfates produced from the reactive uptake of BEPOX are analogues of the previously characterized 2-methyltetrols and organosulfates of isoprene, consistent with the hypothesis that the reactive uptake of IEPOX is likely responsible for some of the observed enhancements of isoprene SOA under low-NO_x and acidic conditions (*12*).

BEPOX is stable in the Teflon bag suggesting that under the experimental conditions described here, wall losses are negligible. Nevertheless, experiments carried out under humid conditions or with acidified walls show immediate uptake of IEPOX to the walls. This may explain why this compound has been difficult to detect.

Calibrations

As detailed in a recent study, the calibration of the CIMS instrument for a specific compound can be estimated from the collision rate constant of the reagent ion (in this case CF_3O^-) with the analyte species (6). The thermal collision rate constant can be estimated from the dipole and polarizability of the analyte species using the parameterization of Su et al.(*13*). The average dipole moment and polarizability were calculated with the B3LYP/6-31G(d) density functional method for the compounds of interest (Table S2) (*14, 15*). Theoretical calibrations show good agreement between the ratio of the calibration obtained for BEPOX, glycolaldehyde and hydroxyacetone (Table S3).

Cis and *trans* conformers of β-IEPOX exhibit very different dipole moments. The CIMS is predicted to be ~37% more sensitive to the *cis* than to the *trans* conformer. The conformation of IEPOX depends on the both the conformation of the ISOPOOH peroxy radical before OH adds and on the rotation about the carbon bond prior to the oxirane formation. Theoretical calculations show that the *cis* conformation of the carbon radical is largely favored over the *trans* conformation. Nevertheless, given the excess energy of the carbon radical, it is unclear that the radical will be sufficiently long-lived to reach an equilibrium structure before it decomposes to IEPOX. In other words the relative rate of formation of the conformers depends on the formation time scale of IEPOX versus the time scale of bond rotation. These experiments provide some constraints. It is non-physical for all the IEPOX to be *trans* as it would result in a yield exceeding 100%. In this study, we assume that IEPOX was entirely in its *cis* conformation. A racemic mixture would increase the yield by about 20%, well within the calibration uncertainty.

Experiments using isotopically-labeled OH are used to derive a calibration for the CID fragments of IEPOX and ISOPOOH. In particular the signal at *m/z*=207 can be associated with the dilabeled epoxide. We derive a ratio for the daughter m/z=187 to parent m/z=207 of 11.34. Using this ratio, the contribution of the epoxide from the parent m/z=205 signal can be removed. The resulting signal corresponds to the peroxide contribution: $m/z\ (205)_{CORRECTED} = m/z\ (205) - 11.34 \times m/z\ (205 \rightarrow 185)$. The ratio of $m/z\ (205)_{CORRECTED}$ to m/z (205 → 63), the characteristic daughter of the peroxide, is then found to be 6.9. With these derived relationships between the characteristic daughters and the parent signals, the calibration for the parent signals previously derived from the dipole moments and polarizabilities can be used to infer the calibration factors for the characteristic daughter ion signals.

MVK and MACR are monitored together in positive ion mode at m/z=89 (via SR4 with n=1). We calibrate for both compounds using native standards (Sigma Aldrich).

CID-Signature of the IEPOX and ISOPOOH

Negative mode

The combined use of CIMS and CID is new and therefore no published database is available against which the observed fragments can be compared. Instead, we build such a data base using synthesis of these or related compounds. Although there are many daughters of m/z=203, the signal at all daughters can be described as a linear combination of two daughters nearly unique to the first and second generation products - m/z=63 and m/z=183 respectively. ISOPOOH makes only a minor contribution to m/z=183: m/z_{183}(ISOPOOH)~ 5% of m/z=63.

The identification of ISOPOOH is supported by the daughter m/z=63. Using photooxidation of 3-methylbutene and 2-methylbutene in a fashion similar to that described in the isoprene study, we "synthesized" in the gas phase related β-hydroxyhydroperoxides. Each gives rise to a m/z=63 daughter analogous to ISOPOOH. This daughter is not seen in either hydroxyaldehydes or polyols.

As illustrated in Fig. S2 and similar to isoprene, the photooxidation of butadiene gives rise to the successive formation of hydroperoxides (loss of negative fragment 63 amu through SR5g) similar to ISOPOOH and epoxides similar to BEPOX (loss of neutral fragment 20 amu SR5b), consistent with our approach.

Positive mode

While the CF_3O^- based CIMS technique remains rare (1-4), PTR-MS instruments are commonly used in chamber and field experiments, motivating the search for a potential fingerprint of IEPOX and ISOPOOH in positive mode.

As previously suggested (*16-18*), ISOPOOH is detectable at m/z=101 (addition of H^+ followed by loss of water). Nevertheless, we find significant contamination of IEPOX at this mass which may have affected previous measurements. Conversely, m/z=119 appears to be mostly representative of IEPOX. Concomitant measurements of both m/z=119 and m/z=101 should provide another proxy to measure the partitioning between

IEPOX and ISOPOOH in field missions. We note, however, that this separation may not be possible with PTR-MS systems which utilize an energetic ion de-clustering stage, as this may push product ions from both compounds to m/z=101. In any case, PTR-MS does not enable to differentiate between IEPOX and ISOPOOH as clearly as negative ion CID-MSMS.

Theoretical method: Formation of β and δ-IEPOX

All stationary points in reactions R2a and R2b and the analogue β1-ISOPOOH reaction have been optimized with the B3LYP/6-31G(d) method. The transition state (TS) between the alkyl radical and the epoxide has a single imaginary frequency at 729 cm^{-1}, 689 cm^{-1} and 676 cm^{-1} for the β1-TS, β4-TS, and δ4-TS, respectively (*19*). As expected, the imaginary mode is a vibration along the OO bond. Intrinsic Reaction Coordinate (IRC) calculations were done in both the forward and backward direction (*20*). We let the IRC calculation run 20 steps (each 0.01 a.u. along the reaction path) in each direction, which was sufficient to connect the TS to the optimized structures. For example, for the β1-channel, the 20 steps in backward reaction led to a structure very close to the optimized alkyl radical. The OO distance in the final IRC step is only 0.02Å longer than the OO distance in the optimized structure. The final structure in the forward direction has the HO group loosely attached and the oxirane is not completely formed. The COC angle is 58° in the last step and is 62° in the optimized β-IEPOX. The CO distance is 1.62 Å whereas it is 1.44 Å in β-IEPOX. We also located a product complex with the HO radical hydrogen bound to the expoxide oxygen atom. With the amount of excess energy available this complex is unlikely to form and is of little importance for the reaction. Similar results are obtained for the β4- and δ4-channel.

We have calculated B3LYP single point energies with the correlation consistent polarized triple zeta (cc-pVTZ) basis set on the B3LYP/6-31G(d) optimized structures and have also optimized each structure with the B3LYP/cc-pVTZ method. The B3LYP/cc-pVTZ and B3LYP/6-31G(d) structures are similar. The B3LYP/cc-pVTZ optimized geometries of the TS has a single imaginary frequency at slightly lower frequency of 704 cm^{-1}, 658 cm^{-1} and 651 cm^{-1} for the β1-TS, β4-TS, and δ4-TS, respectively, in good agreement with the B3LYP/6-31G(d) results. The B3LYP/cc-pVTZ optimized geometries are shown in Figs. 3, S3 and S4 and the B3LYP relative energies are given in Tables S4, S6 and S7. For all three reactions, the B3LYP/cc-pVTZ optimized relatives energies are very close to the B3LYP/cc-pVTZ single point relative energies on the 6-31G(d) structure and within 2 kcal/mol of the B3LYP/6-31G(d) energies.

To corroborate the B3LYP results we have, for the four B3LYP/cc-pVTZ optimized stationary points on the β4-ISOPOOH to β-IEPOX reaction, calculated single point energies with second order perturbation Møller-Plesset (MP2) and the recently developed explicitly correlated coupled cluster (CCSD(T)-F12) methods, as implemented in MOLPRO 2008.1 (21, 22). We have used the VDZ-F12 orbital basis sets of Peterson et al. that have been specifically optimized for use with explicitly correlated F12 methods(*23*). The VDZ-F12 basis sets is of similar size to the aug-cc-pVDZ basis set. Density fitting approximations (*24, 25*) were used in all explicitly correlated calculations using the VDZ/JKFIT and the AVDZ/MP2FIT auxiliary basis sets of Weigend et al. (*26, 27*). We have used the resolution of the identity (RI) auxiliary basis sets of Yousaf et al. for all RI approximations (*28*). In the MP2 calculations we have used used the cc-pVTZ and aug-cc-pVTZ basis sets. We found that the unrestricted MP2 (UMP2) calculation on β4-TS, led to a large spin contamination (S^2 =1.27 with UMP2/aug-cc-pVTZ) which is unreasonable and hence the UMP2 results are not included. Instead we have used the restricted open (ROMP2) for the two radicals and RMP2 for the β4-ISOPOOH to β-IEPOX structures.

The calculated relative MP2 and CCSD(T) energies are given in Table S5. These higher level correlated results for the β4-ISOPOOH reaction corroborate the B3LYP results. The noticeable difference between the B3LYP and correlated results is in the barrier between the alkyl radical and the TS, which is about 10 kcal/mol with B3LYP and CCSD(T)-F12 and about 3-5 kcal/mol with the RMP2 method. The explicitly correlated F12 method with the VDZ-F12 basis set is known to give near basis set limit CCSD(T) results (*22*) and are as such considered to approach chemical accuracy (*29, 30*). These higher level calculations corroborate the B3LYP result, that the reaction to form the epoxide is energetically favorable and proceeds through a small barrier.

Possible interferences from isomers of IEPOX

We have shown in the previous section that the identification of ISOPOOH and IEPOX was supported by CIMS-CID, via their unique fragmentation pattern. Other observations confirm our attribution.

From the ratio of m/z=204 to m/z=203 (largely a measure of the ^{13}C content of the ion), we find that both the first and second generation MW118 compounds have five carbons, consistent with IEPOX formation.

Because of the high yield, the candidate isomers need to be formed from ISOPOOH via a mechanism which incorporates one ^{18}OH while releasing one ^{16}OH. The reaction of OH with ISOPOOH will proceed almost exclusively by addition of OH to the remaining double bond. The measured lifetime of ISOPOOH is completely consistent with this understanding. In a previous section, we showed using quantum mechanical calculations that following the addition of the OH, the energetic barrier to formation of IEPOX lies significantly below the OH+ISOPOOH entrance channel energy. This implies that the lifetime of the highly excited alkylradical HO•ISOPOOH will be very short before fragmentation to the epoxide and OH. To form a peroxy radical (RO_2), many nanoseconds will be required as only 1 in 5 collisions will be with O_2 and few of these will be reactive. Consistent with the lack of formation of the RO_2 following the OH addition to ISOPOOH, we do not observe any dihydroxydihydroperoxide. The ^{18}OH experiments further confirms that the second generation product results from the addition of a second OH radical and, by mass balance, loss of OH. This can be seen in Fig. 2 where the 205 signal (one ^{18}O) is converted mostly to a second generation product with two ^{18}OH (m/z=207). Again, these observations are consistent with the formation of IEPOX.

The isomers of IEPOX which have been previously proposed based on iSOA speciation (*10, 31*) cannot explain our observations (Table S8). However, they may have resulted from IEPOX heterogeneous chemistry (*31*).

Additional mechanisms

Addition of OH on isoprene second double bond

In the main body of the manuscript, we have described the addition of OH onto the double bond which does not carry the methyl group. Addition also occurs on the other double bond as described below.

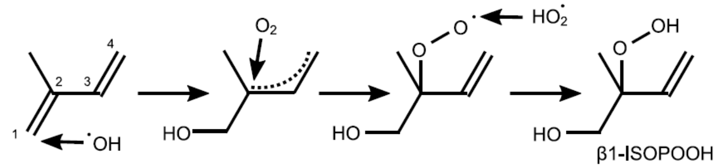

(SR6a)

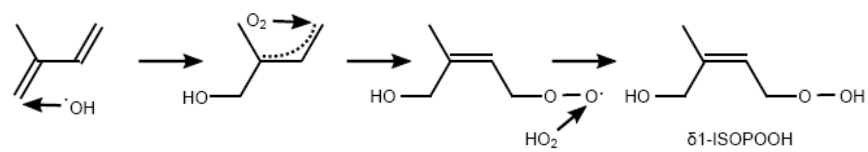

(SR6b)

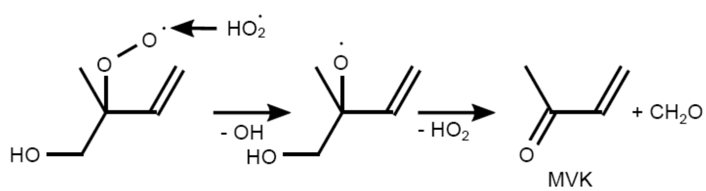

(SR6c)

Given the yield of IEPOX, δ1-ISOPOOH produced by (SR6b) is likely to lead, at least partly, to δ1-IEPOX. This would suggest that OH can add substantially on the side of the double bond bearing the methyl group (~50%).

Addition of OH on carbons 2 and 3 (cf. SR6a) is less than 10% and wasn't considered in this study (*32*).

Fate of IEPOX

We investigated this reaction using synthesized BEPOX reacting with labeled ^{18}OH. It appears that the reaction of IEPOX with OH occurs mostly by abstraction of the H α to the alcohol followed by the opening of the oxirane C-O bond.

Five different channels were considered:

- Abstraction of the epoxidic H

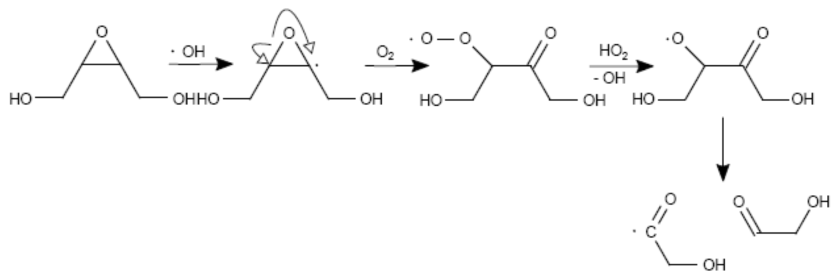

(SR7a)

- Abstraction of the H α to the alcohol followed by reaction with O_2

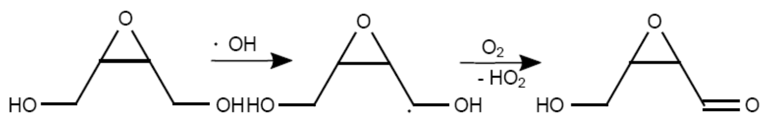

(SR7b)

- Abstraction of the H α of the alcohol followed by opening of C-O bond of the oxirane

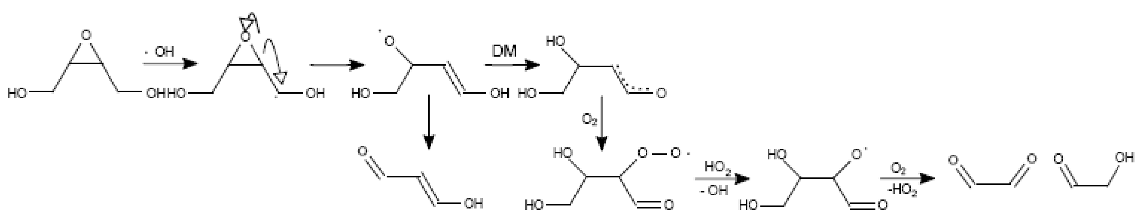

(SR7c)

.

DM refers to the mechanism first suggested by Dibble (*33, 34*).

- Abstraction of the H α of the alcohol followed by opening of C-C bond of the oxirane

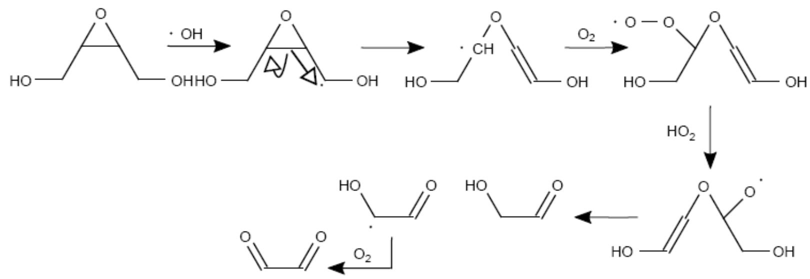

(SR7d)

- Addition of OH to the oxirane

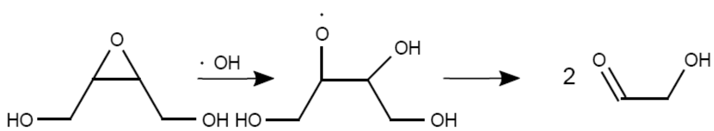

(SR7e)

The only mechanism yielding singly labeled glycolaldehyde is SR7e. Very little signal is recorded at this mass suggesting that OH is not incorporated into the oxirane. This is also consistent with the absence of dilabeled hydroxyacetone and glycolaldehyde in the isoprene + ^{18}OH experiments.

The signal recorded at m/z=187 corresponding to the product of SR7b also represents a minor contribution to the total signal. This is consistent with the unlabeled isoprene experiment where little signal is recorded at m/z=201, the analog of m/z=187 in the isoprene system.

SR7a (*35*), SR7c and SR7d all yield non-labeled glycolaldehyde and are difficult to distinguish directly because of the BEPOX symmetry. However, data from ^{18}OH + isoprene suggest high yields of both singly-labeled hydroxyacetone and glycolaldehyde from IEPOX photoxidation. This suggests that the analogue of SR7a for isoprene is not the main oxidation channel, as no glycolaldehyde can result from this channel. Furthermore if SR7a is an important decomposition pathway, dilabeled glycolaldehyde from δ4-IEPOX would be formed. However, dilabeled glycolaldehyde is not observed.

SR7c and SR7d are mostly indistinguishable and further studies are required to investigate these mechanisms in more detail. It is suggested here that the reaction of IEPOX with OH occurs mostly by abstraction of the H α to the alcohol followed by the opening of the oxirane C-O bond (SR7d**).** The signal recorded at m/z=91 in PTR-MS mode may be associated with the formation of the enol, 3 hydroxy-2-propenal.

Furthermore the analogue of SR7c applied to the IEPOX seems thermodynamically unfavorable as it requires a rearrangement which involves the formation of a primary radical from a secondary radical.

δ1-IEPOX cannot undergo SR7d and its fate remains uncertain. For simplicity we have assumed in our kinetic model and in the proposed GEOS-CHEM mechanism that δ1 - IEPOX shares the fate of δ4 - IEPOX, yielding hydroxyacetone.

Kinetic mechanism

In our simulations of the laboratory experiments, we used a simplified chemical scheme focusing on the first few hours. The different isotopes for each species are explicitly treated but we neglect any kinetic isotope effect on the reaction rate constants or the yields of the reactions.

Cross reactions of peroxy radicals are treated using a class approach (*36-38*). This approach was modified to account for the possibility of homomolecular biradical cross-reactions. The reaction of a peroxy radical (RO_2) with a class of peroxy radical CLO_2 is defined as:

$$\frac{d[RO_2]}{dt} = -k_{CO_2}^{RO_2}[RO_2][CO_2]\left(1 + \frac{[RO_2]}{[CO_2]}\delta(RO_2, CLO_2)\right)$$

where δ(x,y) is the Dirac function. A simplified scheme is used to treat the products of the RO_2+RO_2 channel. This approximation is justified as the experiment was designed to limit the role of these reactions.

Peroxy radicals formed by the reaction of OH with isoprene were divided into two classes: β (70%) and δ peroxy radicals (30%). Addition of OH on the internal carbons are neglected as they account for less than 10% of the carbon (*6*).

The expected product of R1c for the δ channels (isomer of 1-hydroxy-4-oxo-2-methylbut-2-ene) is not observed in large yields. Therefore we assume that R1c is only occurring for the β peroxy radicals, consistent with the formation of MVK and MACR. The fraction of β peroxy radicals undergoing analogue of R1c is ~17%. The ratio between the yields of MVK and MACR is assumed to be equal to the one derived under high NO_x conditions.

In addition to the ^{16}OH regenerated from the VOC photooxidation, an additional conversion of ^{18}OH to ^{16}OH of ~$7s^{-1}$ takes place in our experiments. A minor fraction of this conversion can be attributed to the reaction of OH with water (13%)(*39*). Experiments at reduced oxygen concentration suggest that the reaction of OH with O_2 could account for the bulk of this conversion (k~$1.3x10^{-18}$ cm^3/(molec.s))(*40*). For the conditions of this experiment, the production of ^{18}OH from hydrogen peroxide photolysis, ~ 2.2 x 10^8 s^{-1} ($[H_2O_2]$ = 2ppmv) largely exceeds the conversion of ^{18}OH to ^{16}OH.

Uncertainties regarding the fate of IEPOX as described in the previous section have little effect on our conclusions since channels SR2c and SR2d share the same products.

Comparison between modeled and measured ISOPOOH and IEPOX are shown in Figs S5 (Experiment 1, cf. Table S1) and S6 (Experiment 3). For experiment 2, modeled ^{16}OH is about 4.5 x 10^5 molec/cm^3, ^{18}OH 1.8 x 10^6 molec/cm^3, $H^{16}O^{16}O$ 2x10^9 molecules/cm^3, $H^{16}O^{18}O$ 1.1x10^8 molecules/cm^3 and $H^{18}O^{18}O$ 2.8x10^9 molecules/cm^3.

GEOS-CHEM

GEOS-CHEM v8.01.04 (http://www-as.harvard.edu/chemistry/trop/geos/) driven by assimilated meteorological observations from the Goddard Earth Observing System (GEOS-4) of the NASA Global Modeling and Assimilation Office (GMAO) (*41*) is used to assess the global impact of the isoprene chemistry described herein. The model is run with a spatial resolution of 4° latitude and 5° longitude and 30 vertical levels (22 in the troposphere).

Isoprene emissions are taken from the Global Emission Inventory Activity (GEIA) inventory (*42*). The default chemical mechanism is updated to incorporate recently proposed modification to the high NOx chemistry (6) as well as the low-NOx regime derived in this study (Table S9).

Dry deposition for IEPOX and ISOPOOH is modeled using H_2O_2, while hydroxymethylhydroperoxide (HMHP) parameters are used to model their wet deposition.

A model spin-up of 15 months is done before the results are retained. The results presented in this study are for northern hemisphere summer 2002 and northern hemisphere winter 2001. Isoprene emissions from GEIA are scaled in GEOS-CHEM so that the flux of isoprene to the atmosphere is ~342 TgC/yr. This yields a yearly IEPOX formation of ~65 TgC/yr. Estimates of isoprene emissions range from 250 – 750 TgC/yr. Assuming that IEPOX formation scales with isoprene emissions, this leads to our global estimate of yearly production of IEPOX: 95±45 TgC/yr (167 Tg/yr).

The formation of IEPOX from isoprene is predicted to be asymmetric with a larger yield in the southern hemisphere (Fig. S7). More than 60% of IEPOX is formed in the tropics (-15°- +15°) reflecting the influence of anthropogenic activities on the chemistry of isoprene.

Field measurements

TC4

The NASA Tropical Composition, Cloud and Climate Coupling (TC4) mission was designed to investigate the atmospheric structure, properties, and processes in the tropical troposphere. This mission, based out of San Jose, Costa Rica, was conducted during July and August 2007 and consisted of coordinated flights between several NASA aircraft including the DC-8, ER-2, and WB-57. Two Caltech CIMS instruments (single quadrupole instrument and the Varian tandem-MS instrument) were deployed on the DC8.

Low-level legs were flown over the Columbian jungle during several flights. During these legs large signals at m/z=203 were observed with the single quadrupole instrument. Quantification of ISOPOOH and IEPOX is not possible due to uncertainties regarding the ion transmission efficiency for the quadrupole at these high masses as well as the inability of the single quadrupole to separate these mass analogues. The tandem-MS did not monitor m/z=203 during this experiment.

ARCTAS

The primary scientific focus of the 2008 summer NASA Arctic Research of the Composition of the Troposphere from Aircraft and Satellites (ARCTAS) mission was to study boreal forest fire emissions. ARCTAS was a NASA contribution within the greater Third International Polar Year effort (POLARCAT). The NASA DC-8 aircraft was based in Cold Lake, Alberta during the summer phase of ARCTAS, with nine total flights: two transit flights between Cold Lake and Southern California, four local flights from Cold Lake, two flights between Cold Lake and Thule, Greenland, and one local flight from Thule. More information about the ARCTAS mission, including details of the DC-8 instrument payload and an overview of the mission scientific objectives, is available at http://www.espo.nasa.gov/arctas/ .

Two Caltech-CIMS instruments were flown aboard the DC-8 during ARCTAS: the single quadrupole (*3*) and the triple quadrupole (identical to the instrument in the chamber). The triple quadrupole was operated exclusively in CID-MSMS mode while in flight. Both flight instruments monitored m/z=203, though the tandem MS did so for only five of the nine flights.

A subset of the m/z=203 daughters (m/z=63, m/z=85, m/z=137, m/z=203) were measured by the tandem MS for the last five flights of summer ARCTAS. By assuming that the only source of m/z=203 is ISOPOOH and IEPOX, we can infer ISOPOOH and IEPOX respective signals from the flight data. As discussed in the text, ISOPOOH•CF_3O^- was determined to be the source of m/z=63 daughter ion in the chamber experiments. The m/z=183 daughter ion, used in the chamber study as the fingerprint for IEPOX, was not measured during flight. Signal potentially attributable to IEPOX was determined for the flight data by removing the ISOPOOH contribution to the m/z=137 daughter ion signal, using the relationship between the m203 daughters derived from an OH + isoprene chamber experiment where the aircraft tandem MS instrument monitored all relevant m203 daughter masses:

$$\mathbf{(m/z = 203 \rightarrow 137) = (1.49 \pm 0.03) \times (m/z = 203 \rightarrow 63) + (1.43 \pm 0.03) \times (m/z = 203 \rightarrow 183)}$$

where the coefficients and 2σ uncertainties (of the fit) are obtained from a multivariate linear regression.

Both tandem MS instruments sampled from the same chamber during this calibration experiment. By determining the IEPOX contribution to the m/z =203 → 137 ion signal in terms of the m/z =203 → 183 ion signal and also determining the scaling factor between the m/z =203 → 183 ion signals of the two instruments, the IEPOX sensitivity used for the chamber experiments can be applied to the ARCTAS data to obtain *in situ* IEPOX mixing ratios. Determination of *in situ* ISOPOOH mixing ratios required only obtaining the scaling factor between the m/z =203 → 63 ion signals of the two instruments before applying the ISOPOOH sensitivity used for the chamber experiments.

The possibility of mass interferences at m/z=203 *in situ* precludes the definitive attribution of the m/z=203 signal, in its entirety, to ISOPOOH and IEPOX. One known interferent at m/z=203 was identified from data not yet published from a chamber study of the OH oxidation of 2-Methyl-3-Buten-2-ol (MBO). The MBO oxidation product at m/z=203 yields no daughter ion at m/z=63 but does yield a daughter ion mass at m/z=137. Consequently, the presence of MBO oxidation products may influence the calculated ARCTAS IEPOX mixing ratios, but not the ARCTAS ISOPOOH mixing ratios. We currently know of no mass interferences for the m/z=63 daughter ion of m/z=203. In recognition of the potential for interferences, however, the ARCTAS data for ISOPOOH and IEPOX will be hereafter referred to as ISOPOOH_flt and IEPOX_flt, respectively, to distinguish the *in situ* data from the chamber data.

Both ISOPOOH_flt and IEPOX_flt were observed during four of the last five ARCTAS flights, as shown in Fig. S8. All of the ISOPOOH_flt and most of the IEPOX_flt were detected below 1.5 km above ground level (Fig. S9). The highest mixing ratios of both ISOPOOH_flt and IEPOX_flt during the mission, 1.2 ppbv and 3.4 ppbv respectively, were encountered while flying 0.7 km above ground level at 40.7319° N, 122.0492° W. Signal for ISOPOOH_flt was always accompanied by IEPOX_flt signal, but IEPOX_flt was observed without concurrent ISOPOOH_flt signal, consistent with IEPOX having a significantly longer lifetime than ISOPOOH.

Figures

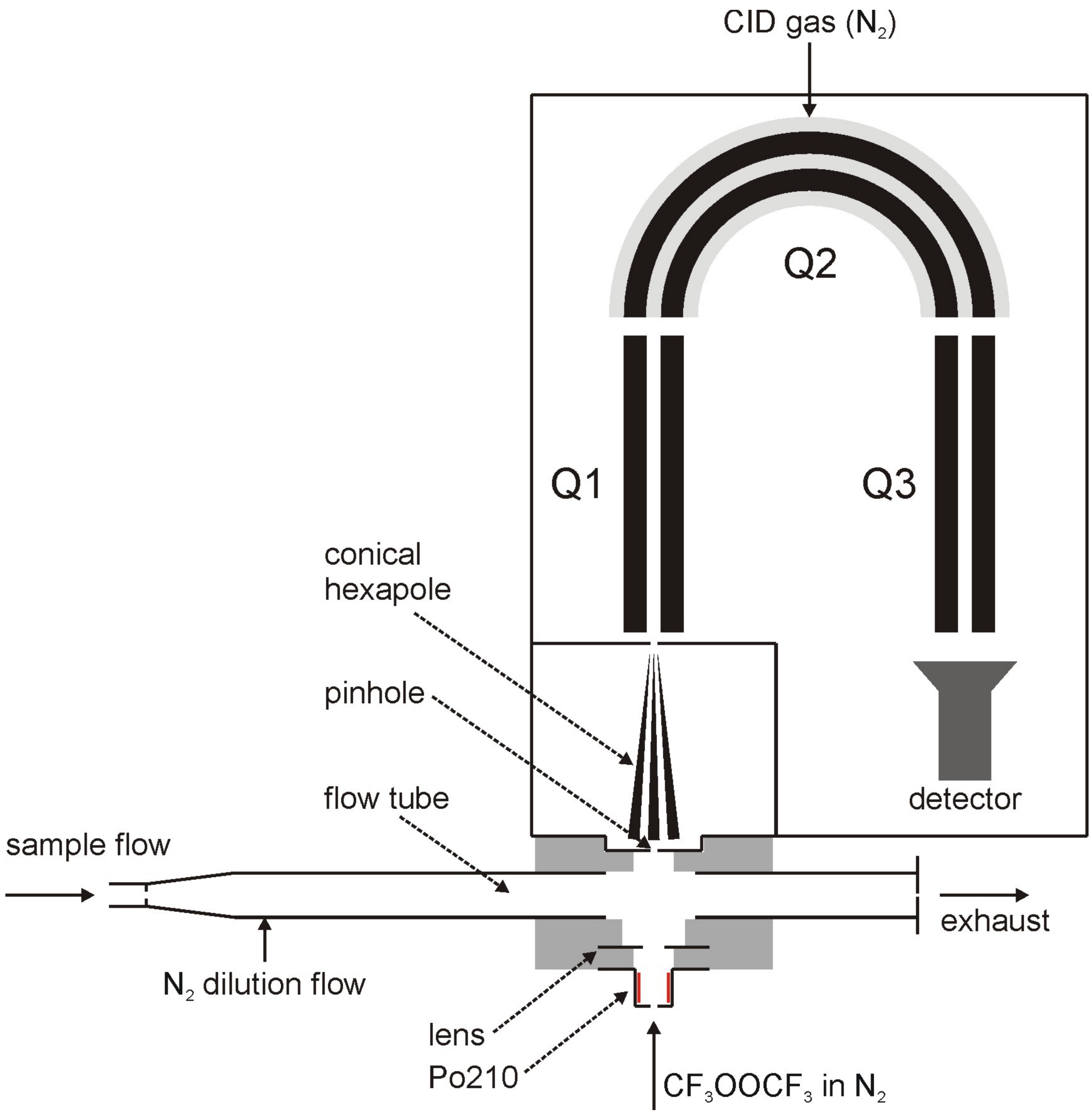

Figure S1 Schematic diagram of the Caltech Chemical Ionization Mass Spectrometer (CIMS).

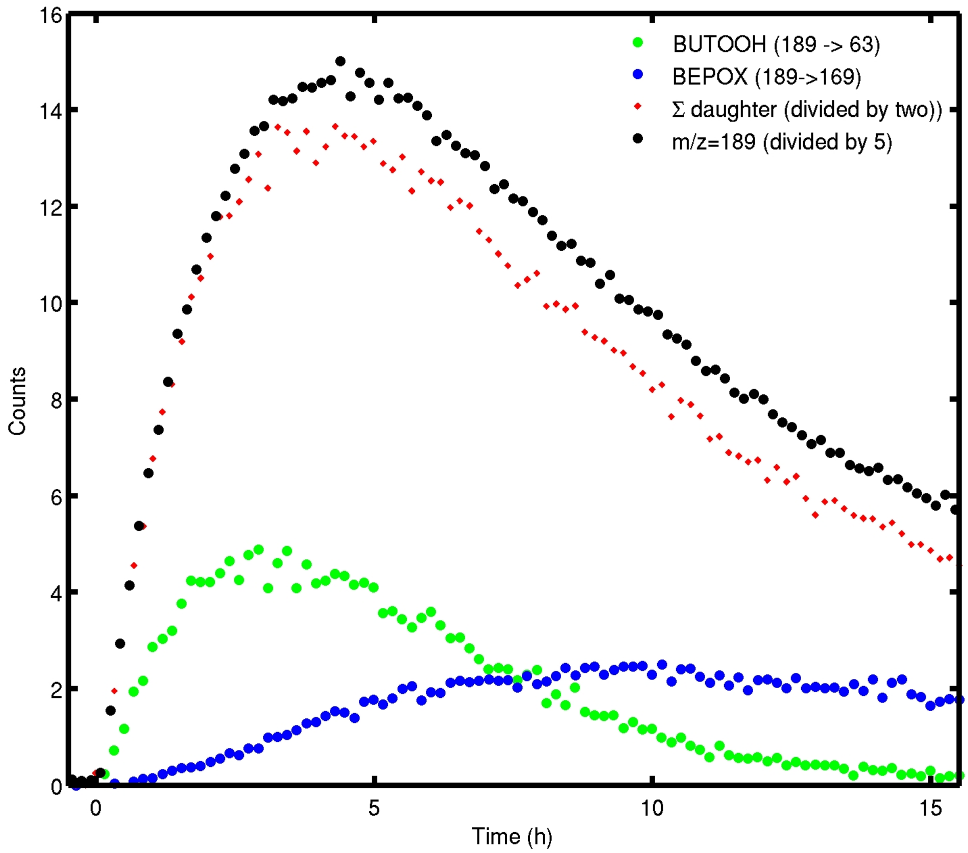

Figure S2 Following the time when the photolysis of H_2O_2 (initially 1 ppmv) begins (t=0), we observe the formation of BUTOOH and then BEPOX together detected at m/z=189 (black). Tandem mass spectroscopy provides for separation of the m/z=189 signal: BUTOOH (green) is observed as the m/z=63 daughter while BEPOX (blue) is observed as the m/z=169 daughter. The sum of the measurable daughters of m/z=189 (red) correctly captures the profile of the parent signal.

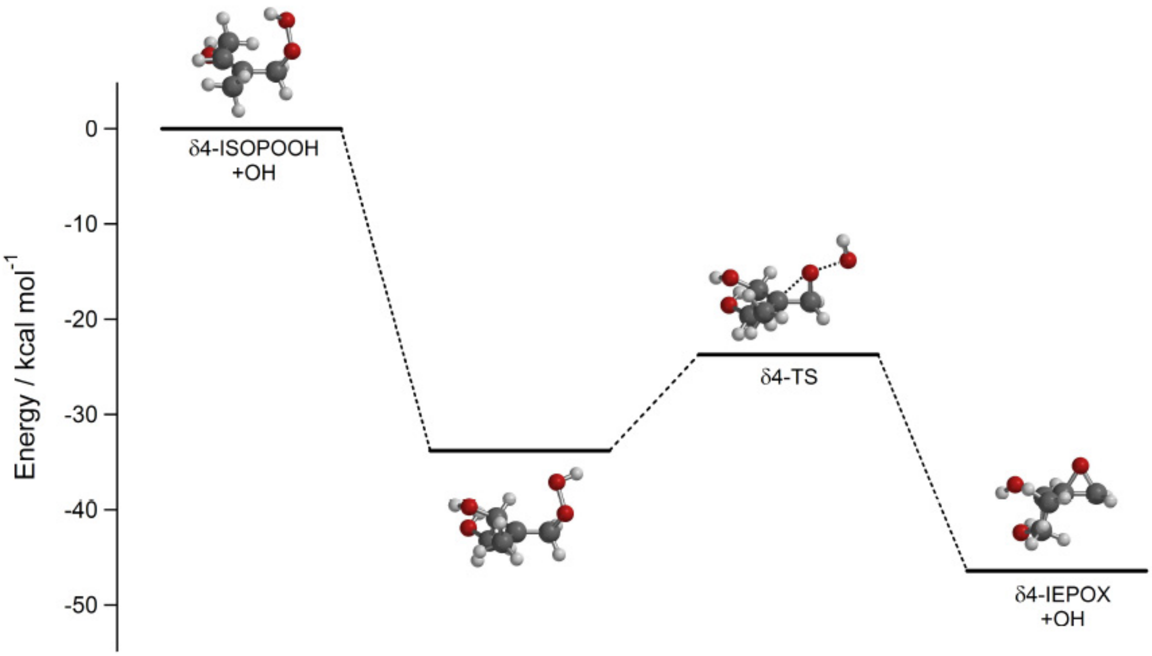

Figure S3 Relative energies of the B3LYP/cc-pVTZ optimized geometries for the formation of δ4-IEPOX from δ4-ISOPOOH.

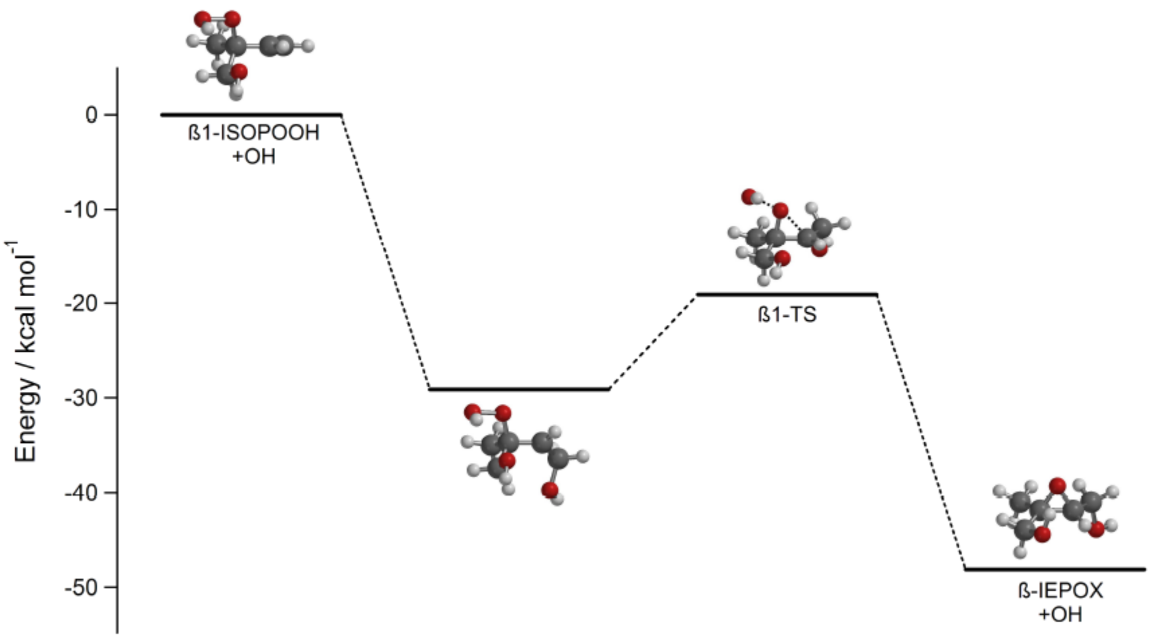

Figure S4 Relative energies of the B3LYP/cc-pVTZ optimized geometries for the formation of β-IEPOX from β1-ISOPOOH.

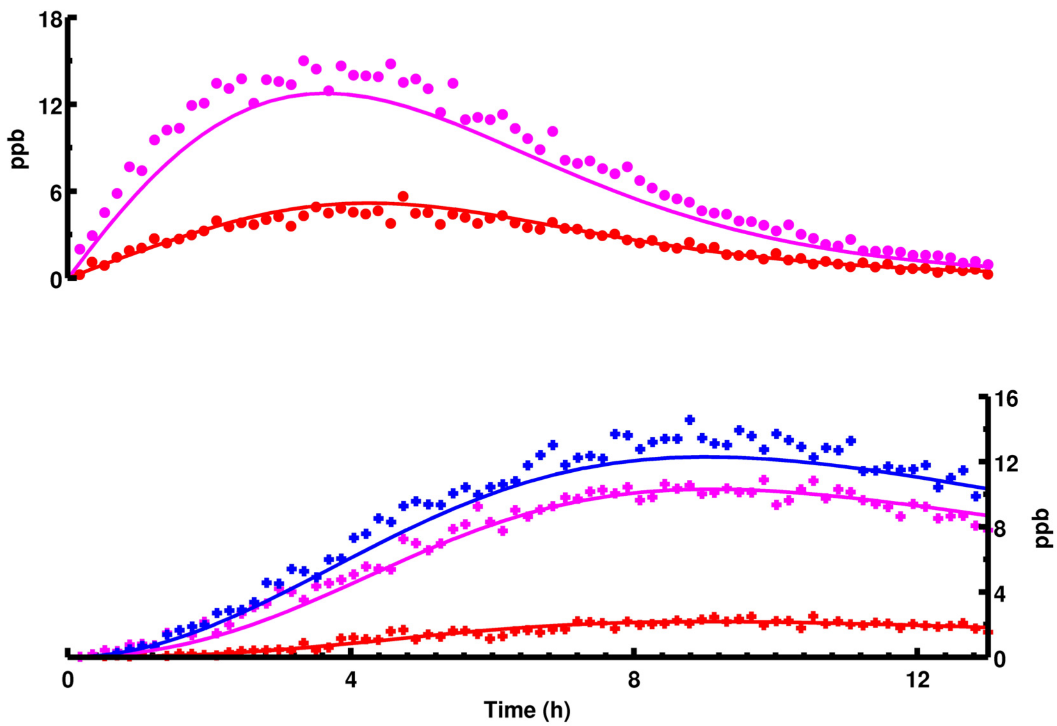

Figure S5 Same as Fig. 2 for Exp 1.

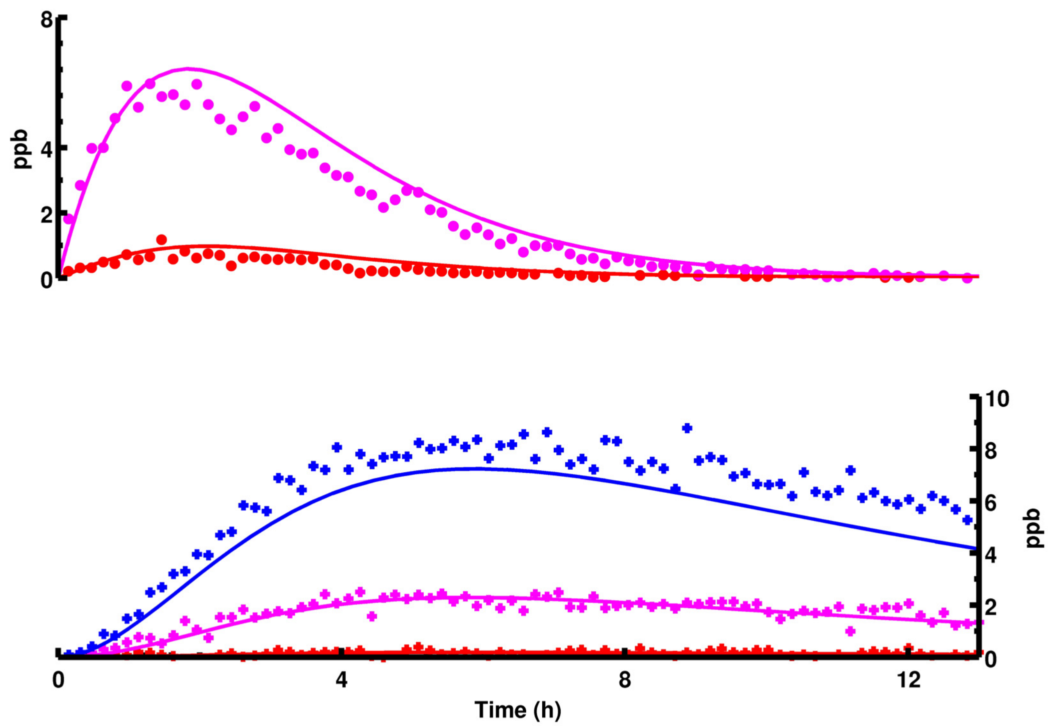

Figure S6 Same as Fig. 2 for Exp 3

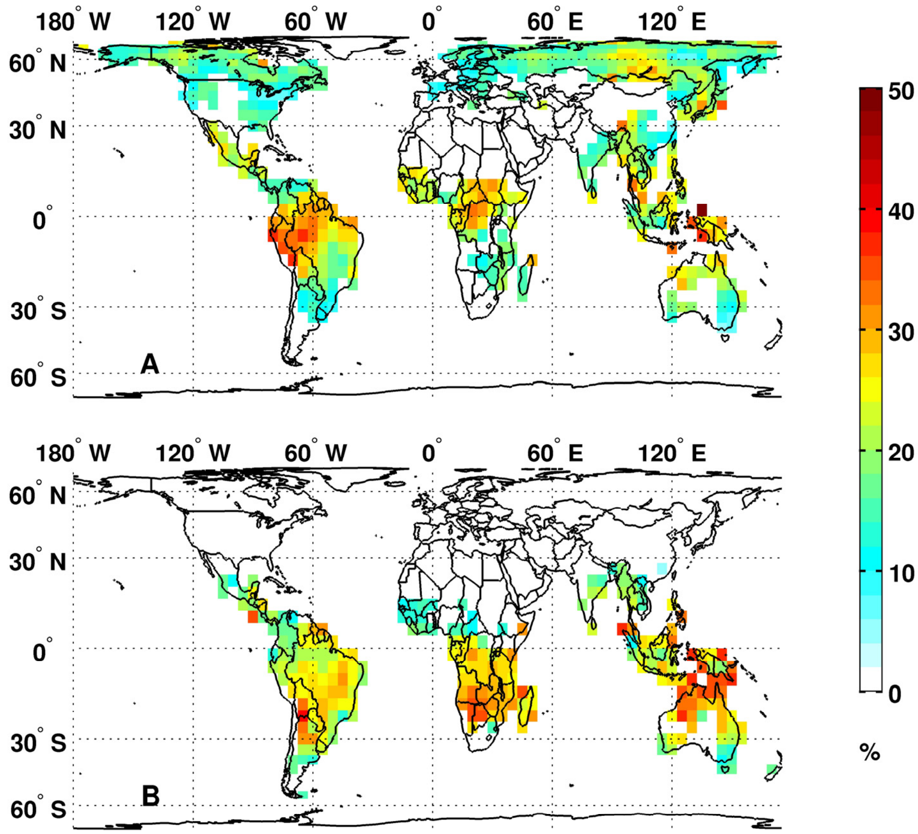

Figure S7 Modeled yield of IEPOX from the reaction of isoprene + OH in the planetary boundary layer. Grid cells where isoprene mixing ratio is lower than 50 pptv are not shown.

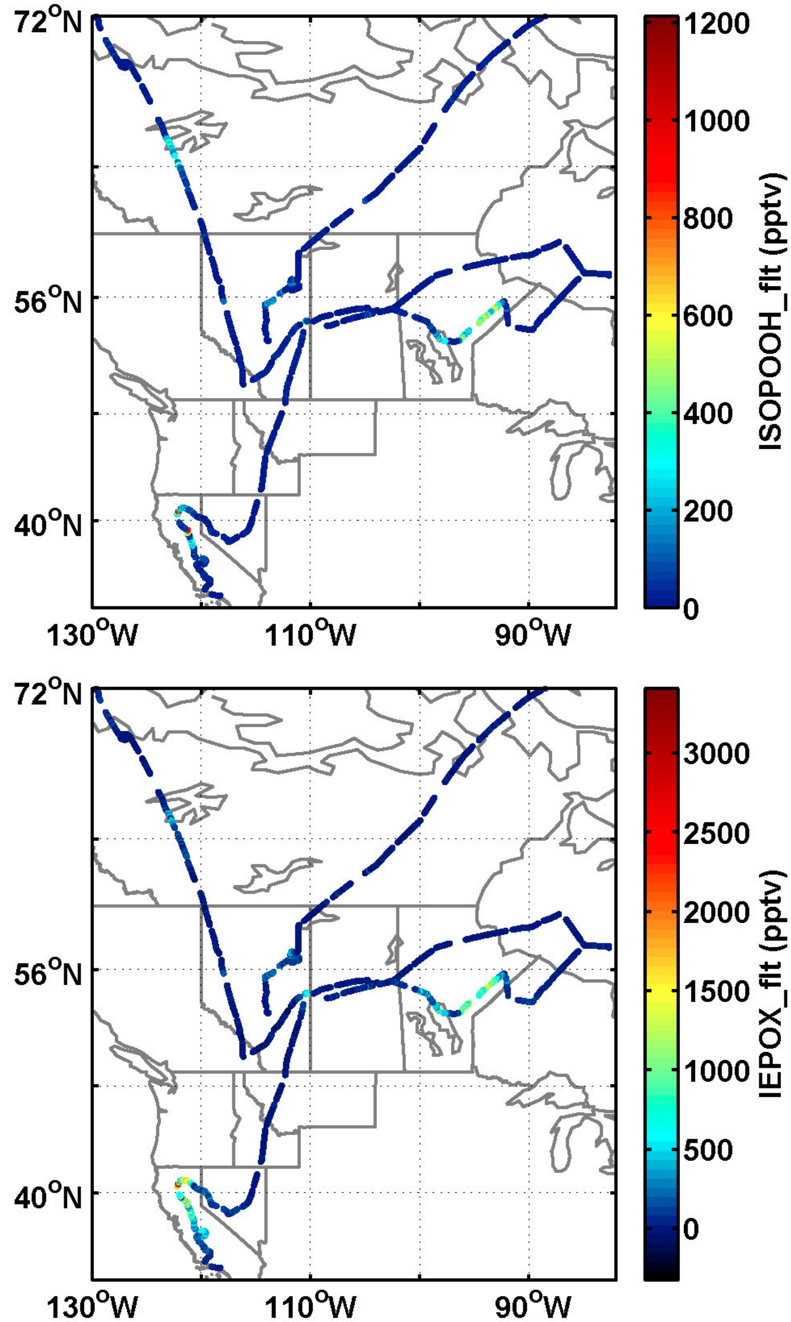

Figure S8 Flight tracks for 2008 summer ARCTAS flights on July 5th, 8th, 10th, and 12th indicating the location of data and the mixing ratio for ISOPOOH_flt (top panel) and IEPOX_flt (bottom panel).

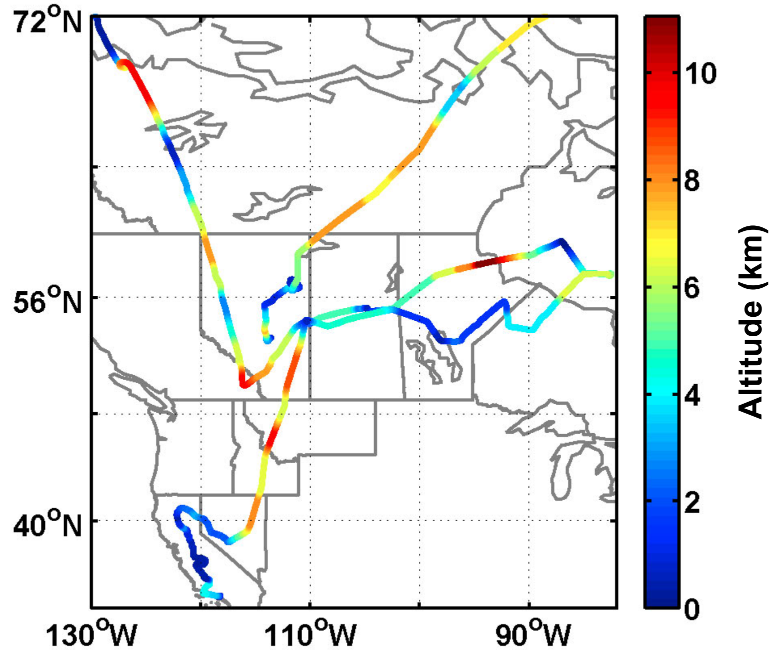

Figure S9 Flight tracks for 2008 summer ARCTAS flights on July 5th, 8th, 10th, and 12th with color indicating the altitude of the DC-8 aircraft

Tables

Table S1 Initial conditions (in ppb)

Experiment	Isoprene	$H^{18}O^{18}OH$	$H^{18}O^{18}OH$	$H^{16}O^{16}OH$	NO_x
Exp 1	70	1700	57.2	3.5	1.3
Exp 2	23.5	1750	58	3.76	.77
Exp 3	20.9	2860	94	5.9	.1

Table S2 Theoretical weighted average dipole moments (μ) and polarizabilites (α) for conformers with abundance greater than 1%. *Cis* and *trans* refer to the position of the CH_2OH group with respect to the plane of the oxirane.

Compound	μ (D)	α ($Å^{-3}$)
β – IEPOX (*cis*)	2.47	8.98
β – IEPOX (*trans*)	1.00	9.01
δ1 – IEPOX	2.39	9.98
δ4 – IEPOX	2.30	8.93
β1 – ISOPOOH	2.19	9.44
β4 – ISOPOOH	2.20	9.44
δ1 – ISOPOOH	2.85	9.63
δ4 – ISOPOOH	3.34	9.66
BEPOX (*cis*)	2.71	7.52
BEPOX (*trans*)	0.55	7.47
(2Z)-but-2-ene-1,4-diol	2.93	7.28
but-3-ene-1,2-diol	2.29	7.21
2-methylbut-3-ene-1,2-diol	2.01	8.79
3-methylbut-3-ene-1,2-diol	2.30	8.76
(2Z)-2-methylbut-2-ene-1,4-diol	2.98	8.98

Table S3 Comparison of the experimental and theoretical calibration for three representative compounds

Compound	Theoretical calibration (normalized counts/pptv)	Experimental calibration (normalized counts/pptv)
BEPOX (*cis*)	2.0×10^{-4}	2.0×10^{-4}
Hydroxyacetone	2.7×10^{-4}	2.6×10^{-4}
Glycolaldehyde	2.2×10^{-4}	2.3×10^{-4}

Table S4 Calculated relative energies (kcal/mol) of the stationary points in the β4-ISOPOOH to β-IEPOX reaction (R2a and Fig. 3).

Species	B3LYP/6-31G(d)	B3LYP/cc-pVTZ//B3LYP/6-31G(d)	B3LYP/cc-pVTZ
β4-ISOPOOH	0	0	0
Alkyl radical	-32.9	-30.4	-30.6
β4-TS	-21.1	-19.7	-20.0
β-IEPOX	-47.8	-47.4	-47.4

Table S5. Calculated relative energies (kcal/mol) of the stationary points in the β4-ISOPOOH to β-IEPOX reaction (R2a and Fig. 3).

Species	RMP2/ cc-pVTZ	RMP2/ aug-cc-pVTZ	MP2-F12b/ VDZ-F12	CCSD(T)-F12b/ VDZ-F12
β4-ISOPOOH	0	0	0	0
Alkyl radical	-33.6	-34.1	-34.8	-30.9
β4-TS	-28.7	-31.3	-31.8	-18.2
β-IEPOX	-54.1	-54.6	-55.5	-50.9

a) All single point energies on the B3LYP/cc-pVTZ optimized geometries.

Table S6 Calculated relative energies (kcal/mol) of the stationary points in the δ4-ISOPOOH to δ4-IEPOX reaction (R2b and Fig. S3).

Species	B3LYP/6-31G(d)	B3LYP/cc-pVTZ//B3LYP/6-31G(d)	B3LYP/cc-pVTZ
δ4-ISOPOOH	0	0	0
Alkyl radical	-37.4	-33.9	-33.8
δ4-TS	-25.9	-23.7	-23.7
δ4-IEPOX	-48.1	-46.5	-46.4

Table S7 Calculated relative energies (kcal/mol) of the stationary points in the β1-ISOPOOH to β-IEPOX reaction (R2a analog and Fig. S4).

Species	B3LYP/6-31G(d)	B3LYP/cc-pVTZ// B3LYP/6-31G(d)	B3LYP/cc-pVTZ
β1-ISOPOOH	0	0	0
Alkyl radical	-31.8	-29.1	-29.1
β1-TS	-20.6	-19.0	-19.1
β-IEPOX	-48.8	-48.2	-48.1

Table S8 Isomers of IEPOX previously observed in the aerosol phase

Possible isomer	Example	Incompatibility with the measurements
Alkene triols	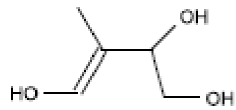	Alkene triol formation has been reported in the aerosol phase(*31*). Proposed formation schemes involve enol/ketone equilibrium with dihydroxycarbonyl (*10*) or acid catalyzed rearrangement of dihydroxyepoxide (*31*). In both mechanisms, formation of alkene triols requires a solvent. The proposed mechanisms cannot take place in the gas-phase. Furthermore, such a compound features a double bond and thus is not consistent with the observed lifetime of the second generation product.
Dihydroxycarbonyl	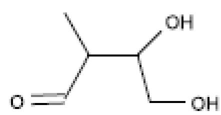	Formation of isobaric dihydroxycarbonyl has previously been proposed through a keto/enol mechanism with the previous isomer (*10*). CIMS has been shown to be sensitive to this class of compounds(*6*). CID of hydroxyacetone and glycolaldehyde standards show a loss of CF_3O^- (m/z=85) exclusively with no measurable loss of HF (20 a.m.u.) or FCO_2^- (fragment at m/z=63). Therefore they cannot account for the formation of daughter m/z=183 which is specific to IEPOX.

Table S9 Low NO_x mechanism for the photooxidation of isoprene

									A x 10^{11} (cm3/(molec.s))	-Ea/R (K)
ISOP	+	OH	→	ISOPOO					2.7	390
ISOPOO	+	HO_2	→	0.880ISOPOOH	+	0.120OH	+	0.047 MACR	0.074	700
				0.073 MVK	+	0.120 HO_2	+	0.120 CH_2O		
ISOPOOH	+	OH	→	IEPOX	+	OH			1.9	390
ISOPOOH	+	OH	→	0.70 ISOPOO	+	0.300 HC5	+	0.300 OH	0.38	200
IEPOX	+	OH	→	IEPOXOO					5.78	-400
IEPOXOO	+	HO_2	→	0.725 HAC	+	0.275 GLYC	+	0.275 GLYX	0.074	700
				0.275 MGLY	+	1.125OH	+	0.825HO2		
				0.200CO2	+	0.375CH2O	+	0.074HCOOH		
				0.251CO						

References

1. L. G. Huey, P. W. Villalta, E. J. Dunlea, D. R. Hanson, C. J. Howard, *J. Phys. Chem.* **100**, 190 (1996).
2. C. Amelynck, N. Schoon, E. Arijs, *Int. J. Mass Spectrom.* **203**, 165 (2000).
3. J. D. Crounse, K. A. McKinney, A. J. Kwan, P. O. Wennberg, *Anal. Chem.* **78**, 6726 (2006).
4. C. Amelynck, A. M. Van Bavel, N. Schoon, E. Arijs, *Int. J. Mass Spectrom.* **202**, 207 (2000).
5. A. Hansel *et al.*, *Int. J. Mass Spectrom. Ion Processes* **149**, 609 (1995).
6. F. Paulot *et al.*, *Atmos. Chem. Phys.* **9**, 1479 (2009).
7. S. P. Sander, *Chemical Kinetics and Photochemical Data for Use in Atmospheric Studies Evaluation Number 15*. (National Aeronautics and Space Administration, Jet Propulsion Laboratory, California Institute of Technology, 2006).
8. D. Cocker III, R. Flagan, J. Seinfeld, *Environ. Sci. Technol* **35**, 2594 (2001).
9. J. R. Skinner, C. H. Wilcoxen, G. J. Carlson, U. S. P. Office, Ed. (1955).
10. J. D. Surratt *et al.*, *J. Phys. Chem. A* **110**, 9665 (2006).
11. J. D. Surratt *et al.*, *J. Phys. Chem. A* **112**, 8345 (2008).
12. J. D. Surratt *et al.*, *Environ. Sci. Technol.* **41**, 5363 (2007).
13. T. Su, W. J. Chesnavich, *J. Chem. Phys.* **76**, 5183 (1982).
14. Spartan'06, *Wavefunction Inc.*, (2006).
15. A. L. Garden *et al.*, *Chem. Phys. Lett.* **474**, 45 (2009).
16. P. Crutzen *et al.*, *Atmos. Environ.* **34**, 1161 (2000).
17. J. Williams *et al.*, *J. Atmos. Chem.* **38**, 133 (2001).
18. C. Warneke *et al.*, *J. Atmos. Chem.* **38**, 167 (2001).
19. Spartan'08, *Wavefunction Inc.*, (2008).
20. M. J. Frisch *et al.*, *Gaussian 03, Revision C. 02*, (2004).
21. H. Werner *et al.*, *MolPro, version 2008.1, a package of ab initio programs*, (2008).
22. D. P. Tew, W. Klopper, C. Neiss, C. Hattig, *Phys. Chem. Chem. Phys.* **9**, 1921 (2007).
23. K. A. Peterson, T. B. Adler, H. J. Werner, *J. Chem. Phys.* **128**, (2008).
24. F. R. Manby, *J. Chem. Phys.* **119**, 4607 (2003).
25. H. J. Werner, T. B. Adler, F. R. Manby, *J. Chem. Phys.* **126**, (2007).
26. F. Weigend, *Phys. Chem. Chem. Phys.* **4**, 4285 (2002).
27. F. Weigend, A. Kohn, C. Hattig, *J. Chem. Phys.* **116**, 3175 (2002).
28. K. E. Yousaf, K. A. Peterson, *J. Chem. Phys.* **129**, (2008).
29. J. R. Lane, H. G. Kjaergaard, *J. Phys. Chem. A* **111**, 9707 (2007).
30. E. Vohringer-Martinez *et al.*, *Science* **315**, 497 (2007).
31. W. Wang *et al.*, *Rapid Commun. Mass Spectrom.* **19**, 1343 (2005).
32. J. Fan, R. Zhang, *Environ. Chem.* **1**, 140 (2004).
33. T. S. Dibble, *J. Phys. Chem. A* **108**, 2199 (2004).
34. T. S. Dibble, *J. Phys. Chem. A* **108**, 2208 (2004).
35. A. P. Meleshevich, *Russ. Chem. Rev.* **39**, 213 (1970).
36. S. Madronich, J. G. Calvert, *J. Geophys. Res.* **95**, (1990).
37. M. E. Jenkin, S. M. Saunders, M. J. Pilling, *Atmos. Environ.* **31**, 81 (1997).

38. S. M. Saunders, M. E. Jenkin, R. G. Derwent, M. J. Pilling, *Atmos. Chem. Phys* **3**, 161 (2003).
39. M. K. Dubey, R. Mohrschladt, N. M. Donahue, J. G. Anderson, *J. Phys. Chem. A* **101**, 1494 (1997).
40. G. D. Greenblatt, C. J. Howard, *J. Phys. Chem.* **93**, 1035 (1989).
41. I. Bey *et al.*, *J. Geophys. Res.* **106**, 073 (2001).
42. A. Guenther *et al.*, *J. Geophys. Res.* **100**, 8873 (1995).